S.1 Statistical analyses and assessment protocol of AMS measurements

In this study, we employ the most common anisotropy parameters that are used to investigate the nature of magnetic fabrics in LPS.

Lineation (L) is defined as $= \frac{K_{MAX}}{K_{INT}}$ and represents the long shapedness of an AMS ellipsoid (1)

Foliation (F) is defined as $= \frac{K_{INT}}{K_{MIN}}$ and describes the oblateness of the AMS (2)

(Tarling and Hrouda, 1993)

The *corrected degree of anisotropy of magnetic susceptibility (Pj)* (Jelinek, 1981) is defined as

$$Pj = \exp\sqrt{\{2\,[(\eta_{MAX} - \eta m)^2 + (\eta_{INT} - \eta m)^2 + (\eta_{MIN} - \eta m)^2\,]\}} \quad (3)$$

Where η are the natural logarithms of principal susceptibility values (e.g.η_{MAX} = ln K_{MAX}) and $\eta m = = \sqrt[3]{\eta_{MAX} \times \eta_{INT} \times \eta_{MIN}}$

This parameter defines the anisotropic nature of a sample.

The *shape parameter (T)* (Jelinek, 1981)

$$T = \frac{2 \times (\eta_{INT} - \eta_{MAX} - \eta_{MIN})}{(\eta_{MAX} - \eta_{MIN})} \quad (4)$$

can be used to identify an oblate (T = 1 to 0) or prolate (T = -1 to 0) shape of the ellipsoid whilst T = 0 indicates triaxial neutral shape.

The statistical significance of the anisotropy, foliation and lineation were checked for each specimen. For this, we use the parameters *F12* and *F23* based on *F*-statistics for anisotropy (Jelinek, 1977). *F12* values > 4 and *F23* values >10 indicate significant anisotropies (Jelinek, 1977). Whilst *F12* indicates the degree of anisotropy testing in the plane that contains K_{MAX} and K_{INT} *(lineation), F23* represents the plane K_{INT}-K_{MIN} (foliation; Jelinek, 1977). *E12* shows the uncertainty in the direction of K_{MAX} of the magnetic foliation plane and represents the 95% confidence angle for the azimuth of K_{MAX} (Jelinek, 1977; Zhu et al., 2004).

We test a data assessment protocol for the magnetic fabric similar to the one applied by Költringer et al. (2021) that bases on experience in loess research (e.g., Lagroix and Banerjee, 2004). Here, we keep all samples that fulfil criteria of primary aeolian magnetic origin: Samples that show a clearly detectible magnetic lineation and foliation (*F12* > 4; *F23* > 10°) and characteristics "typical" of aeolian magnetic fabrics (sub-horizontal K_{MAX} and about vertical K_{MIN}) with sub-horizontally deposited loess exhibiting K_{MIN} inclination >70°, in which E12 does not exceed 20. F is distinctly higher than *L; Pj* shows a similar trend to *F* indicating that *F* controls the shape of the AMS ellipsoid. Positive *T* values indicate oblate susceptibility ellipsoids that may represent gravitationally dominated primary magnetic fabrics (oblateness may also indicate depositional or compacted material loading). In addition, we reject all samples that exhibited a Pearson correlation coefficient in the range from -0.5 to 0.5 between *F* and *Pj*. Only in case these criteria are fulfilled, and no evidence for post-depositional processes are indicated by stratigraphy, we interpret the magnetic fabric towards reconstruction of palaeo-wind directions.

S.2 Topographic impact to the evolving AMS

To estimate possible topographic impacts to the evolving AMS (e.g. by the dip of the surface on which particles are deposited), we compare our outcomes with those from section with a similar geographic setting as suggested by Hus (2003). For this, we selected the Koblenz-Metternich LPS (Reinders, 1999) that provides a comparable geographic and geomorphological setting with thick southerly exposed Upper Pleistocene loess deposits covering the Lower Middle terrace of the Mosel River close to its confluence with the Rhine River (Reinders, 1999). Here, an impact of the topography to loess deposition to the AMS is reported only for the lowermost section that directly covers the terrace surface (0 to 3.5 m) through a pronounced orientation of K_{MAX} parallel to the strike of the terrace, following the course of the Mosel River from west to east. The younger part of the Metternich LPS consisting mainly of primary aeolian loess shows north or north-southward tendency of K_{MAX} and the orientation of the AMS ellipsoids agrees with the primary sedimentary/magnetic fabric (Reinders, 1999). At the Schwalbenberg, the terrace surface of the Rhine Lower Middle Terrace 1 is located at 79 m a.s.l., 8 m below the base of the RP1 profile. Stereoplots (S1) show no sign of imbrication towards a slope (Rees, 1966; Bradák et al., 2020) as seen elsewhere for partly redeposited loess (Zeeden and Hambach, 2021). Based on our comparison between both LPS (Koblenz-Metternich and Schwalbenberg), we argue that the topography did not influence the AMS in the RP1 profile in a relevant way

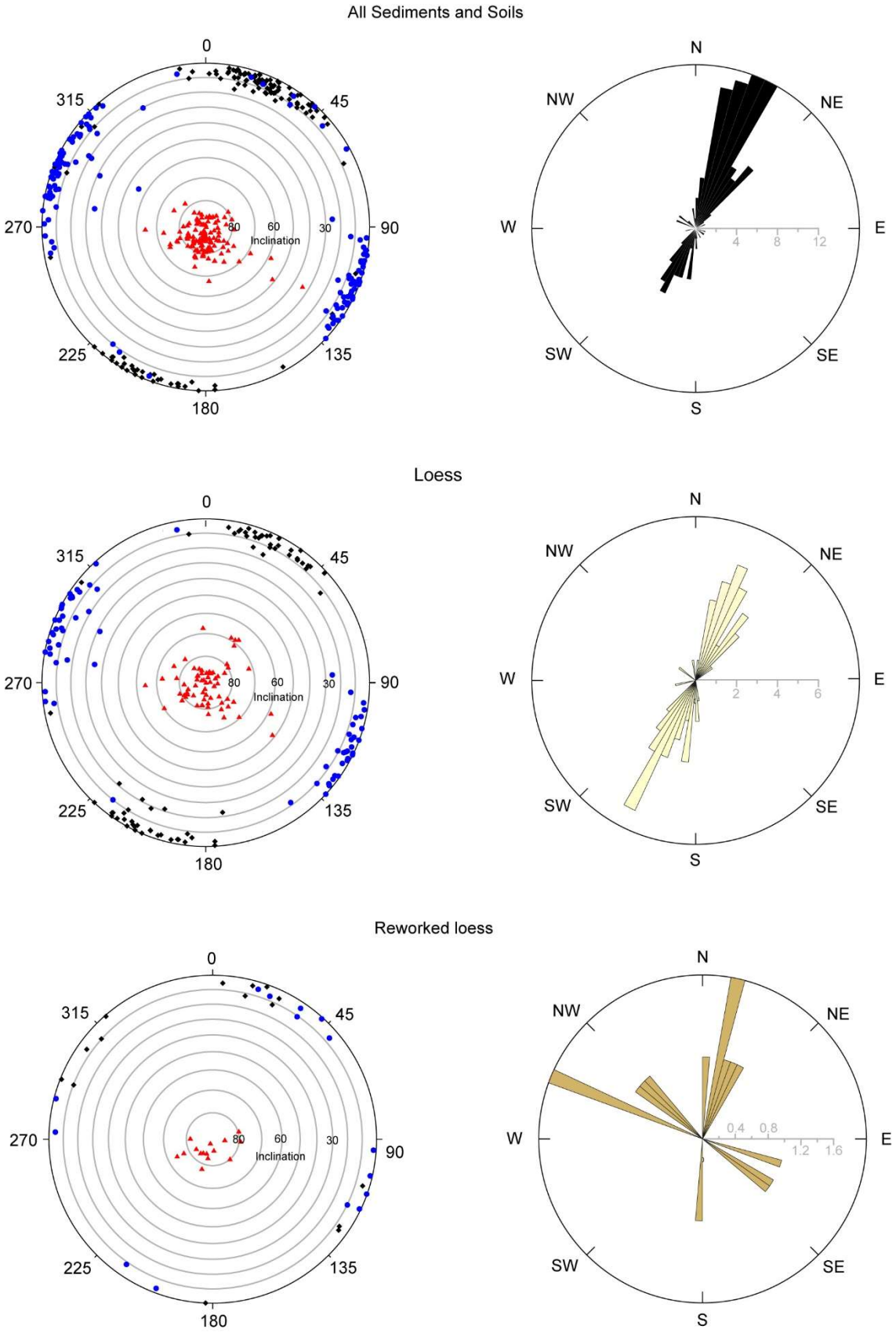

Fig. S1: Stereoplots and rose diagrams for the anisotropy of magnetic susceptibility including all results (primary and secondary magnetic fabric) and those for loess and reworked loess sections. Apart from reworked loess, which shows a random orientation, most samples in loess exhibit a SSW-NNE orientation indicating only limited alteration of the original magnetic fabric (see main text for further explanation).

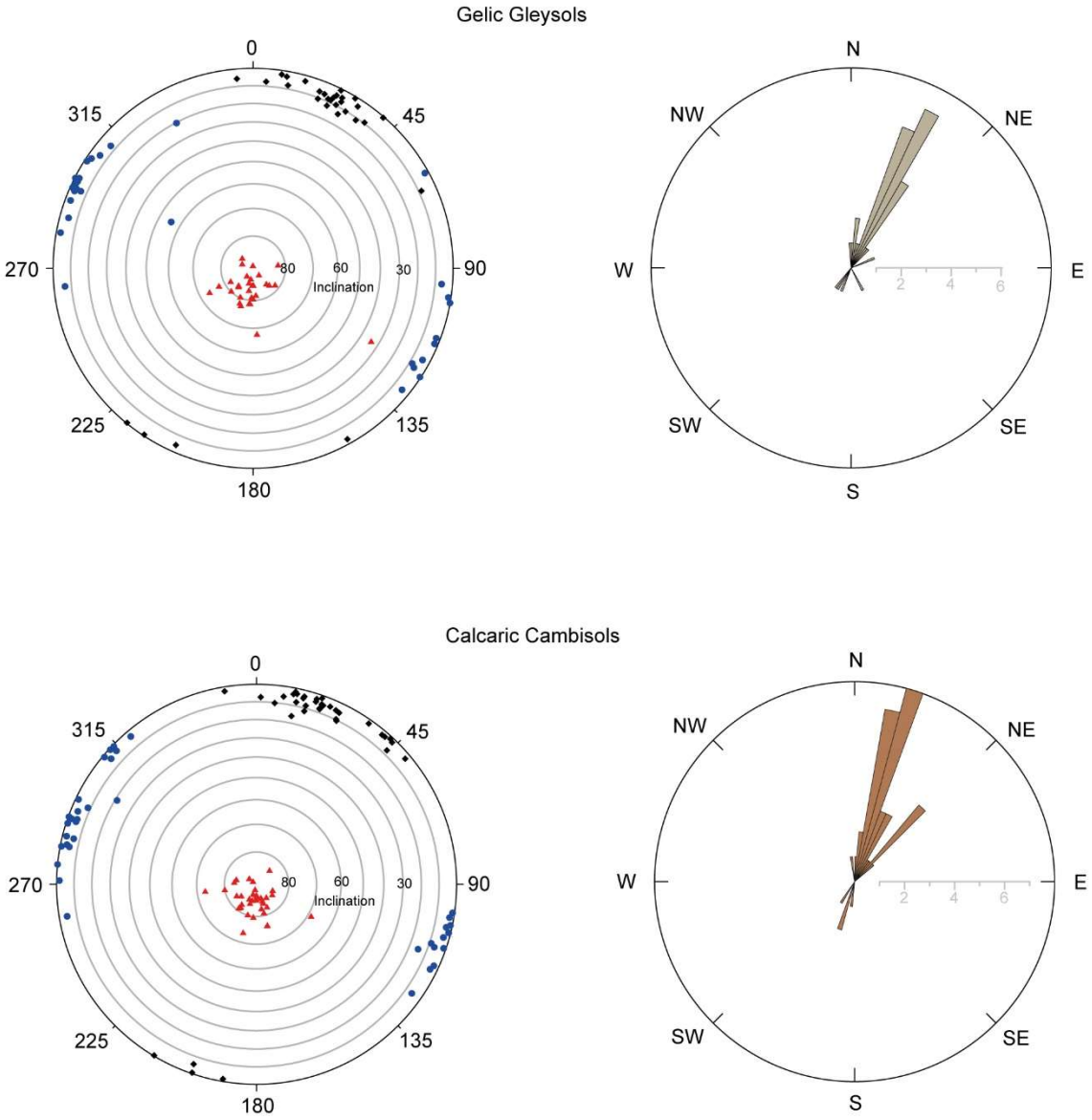

Fig. S2: Stereoplots and rose diagrams for the anisotropy of magnetic susceptibility including all results (primary and secondary magnetic fabric) and those for Gelic Gleysols and Calcaric Cambisols. Gelic Gleysol and Calcaric Cambisol samples are predominantly oriented to NNE. Similar orientations can be observed for samples in Calcaric Cambisols which carry a primary magnetic fabric only (see main text for further explanation). This suggests only minor alteration of the primary magnetic fabric by pedogenesis at the Schwalbenberg for the investigated period. Compared to loess samples, however, Calcaric Cambisols are aligned to NE and not to SW, may suggesting differences in palaeo-wind directions among both sediment/soil types. As we cannot differentiate between both opposing wind directions based on AMS, this remains to be further investigated.

S.3 Additional factors controlling the AMS

Cross plots of anisotropy parameters are frequently used to infer possible palaeoenvironmental processes that dominated during the formation of diverse sediment/soil types (Taylor and Lagroix, 2015; Bradák et al., 2020). Below, we plotted the corrected degree of anisotropy against the foliation. The close correlation between F and Pj indicate foliation control of the anisotropy. Systematically higher *F* and *Pj* values in Gelic Gleysols reflects new alignment of particles through increased pore water contents in these embryonic soils that are prone to water-logging and freeze-thaw cycling effects.

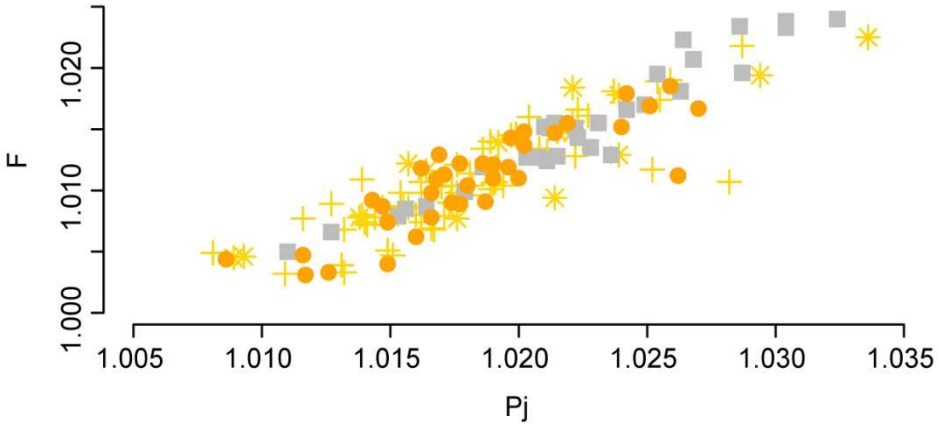

Fig. S3: Relationship between Foliation (*F*) and the corrected degree of anisotropy (*Pj*) including all samples (primary- and secondary magnetic fabric) in Calcaric Cambisols (●), Gelic Gleysols (■), loess (+) and reworked loess sections (✳). Overall, most Gelic Gleysol and some reworked loess samples show the highest degree of *F* and *Pj* indicating new alignment of particles through increased pore water contents.

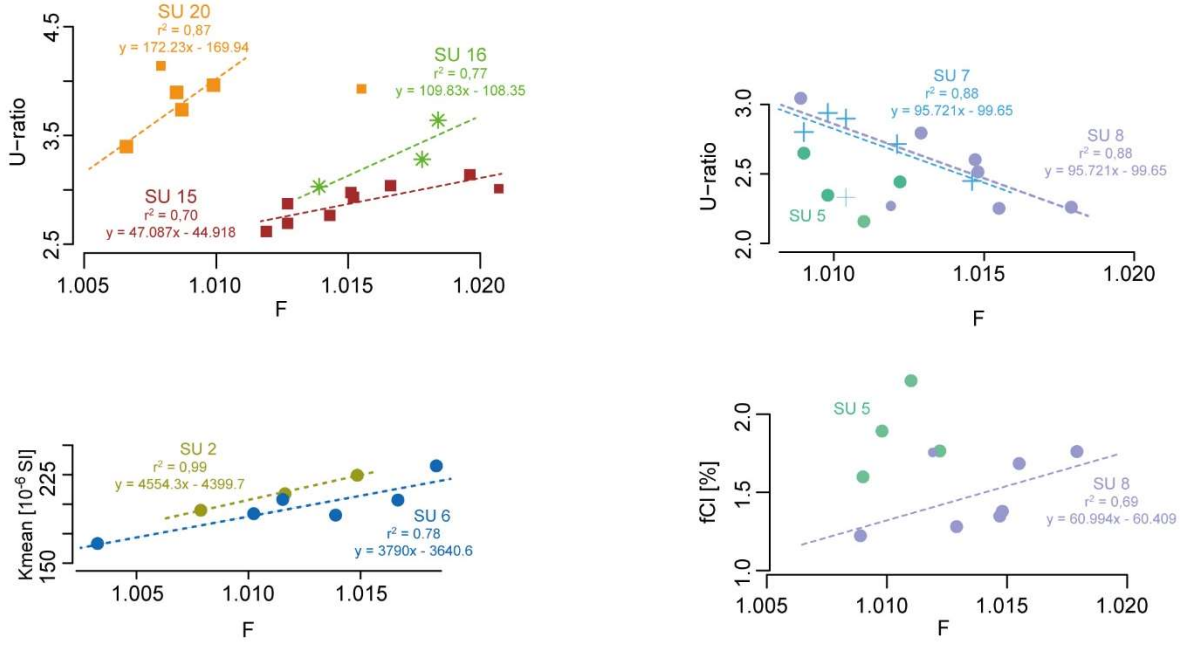

Fig. S4: Linear Relationships between *Foliation* (*F*) and factors potentially influencing the evolving AMS represented by the *U-ratio*, *Kmean* and fCl (values indicated by small symbols are not considered for linear regression analyses). A pronounced positive linear relationship can be observed between F and U in the Upper Section of RP1 (OIS 2) (uppermost graph, left) that are prone to re-alignment of particles by freeze-thaw dynamics (Gelic Gleysols of SU 15, 20) and sediment reworking (SU 16). In contrast, loess of SU 7 and some Calcaric Cambisols (SU 8, SU 5) in the Lower Section of RP1 correlated to OIS 3 show a clear negative linear relationship between U-ratio and F (uppermost graph, right). This indicates that fine silt components, typically deposited during milder interstadials, contribute to the evolving AMS and that the established magnetic fabric can survive secondary alteration at least in relatively weak Calcaric Cambisols and loess layers. For the Lower Section of RP1 characterised by intensive pedogenesis, some Calcaric Cambisols (SU 2 and SU 6) related to GIs 8 and 7 (SU 2, SU 6) indicate secondary alteration of the magnetic fabric likely by neo-formation of ferrimagnetic minerals during soil formation (positive linear relationship between F and Kmean).

High *F* and *Pj* values can also be observed for some reworked loess samples for which re-alignment of particles occurred during their re-deposition. Both mechanisms may lead to grain sorting possibly causing a positive linear relationship between *U-ratio* and *F* (S4 uppermost graph, left). In contrast, a negative linear relationship between *U-ratio* and *F* in weak Calcaric Cambisols and loess units of OIS 3 may indicate that fine silt particles contribute to the evolving AMS and that the primary magnetic fabric may be preserved in these sections. In contrast, a close

relationship between *Kmean* and *F* in stronger developed palaeosols indicates that the primary magnetic fabric is overprinted/erased by neo-formation of ferrimagnetic particles.

S.4 Additional information on sample pre-treatment for isotope analyses

Samples were pre-treated with 0.5 M acetic acid twice to dissolve pedogenic calcite whilst preserving most primary- siliciclastic minerals as well as clay minerals (Asahara et al., 1999). After each acetic acid treatment, the samples were washed three times with Millipore deionised water. The leached material (0.26 g to 0.37 g) was digested using a three-stage process 6 ml 48% HF (AR grade) and 1 ml trace grade 68% HNO_3; 1 ml of trace grade HNO_3 and 5 ml of Millipore water; and finally, 5 ml of 6 M trace grade 37% HCl. In all stages the acids were added to the sample in a Teflon bomb, sealed and heated at 150°C for 8 hours then opened and dried down.

The Sr and Nd fraction of the samples were purified by cation exchange chromatography using Bio Rad analytical grade AG 50 WX8 200-400 mesh hydrogen form to separate the Sr and rare earth elements (REE including the Nd fraction). The Nd was further purified and separated from the other REE by using Eichrom® Ln Resin 100-150 µm. We determined $^{143}Nd/^{144}Nd$ and $^{87}Sr/^{86}Sr$ using an Isotopix Phoenix TIMS device through multi-dynamic analyses.

For instrumental quality control, NIST SRM 987 reference material ($^{87}Sr/^{86}Sr = 0.710255 \pm 0.000013$ at 2σ, n = 5) and JNdi-1 reference material ($^{143}Nd/^{144}Nd = 0.512103 \pm 0.000004$ at 2σ, n =7) were run alongside the samples. A typical internal 2SE for 100 ratios of data for each of the samples is 0.000011 for $^{87}Sr/^{86}Sr$ and 0.000002 ±2SE for $^{143}Nd/^{144}Nd$. For analytical process quality control international CRM material BCR2 (USGS) was leached, digested and analysed alongside the samples. The BCR2 results are $^{87}Sr/^{86}Sr = 0.705068 \pm 0.000056$ at 2σ, n=6 (leached and unleached) and $\varepsilon Nd = -0.24 \pm 0.12$ at 2σ, n=4 (unleached only). In addition, we performed repeats of selected samples throughout the RP1 profile (Table 1 and 2).

Table S1: Additional data on quality control for Nd isotopes (duplicate measurement for selected samples across the RP1 profile).

Measurements	**Identifier**	**Depth [m]**	**Std error %**	**Included ratios**	**εNd**
original	RP1_SrNd_2	0.35–0.40	0.0002	121	-11.15
repeat			0.0002	119	-11.08
original	RP1_SrNd_3	0.80–0.85	0.0003	119	-11.50
repeat			0.0002	121	-11.55
original	RP1_SrNd_11	3.10–3.15	0.0002	122	-10.87
repeat			0.0003	127	-10.86
original	RP1_SrNd_19	4.35–4.40	0.0003	122	-11.98
repeat			0.0002	119	-12.23
original	RP1_SrNd_25	5.00–5.05	0.0002	121	-11.40
repeat			0.0002	122	-11.58

Table S2: Additional data on quality control for Sr isotopes (duplicate measurement for selected samples across the RP1 profile).

Measurements	Identifier	Depth [m]	Std error %	Included ratios	$^{87}Sr/^{86}Sr$
original	RP1_SrNd_11	3.10–3.15	0,0008	152	0.722239
repeat			0,0026	62	0.722143
original	RP1_SrNd_25	5.00–5.05	0,0009	134	0.726556
repeat			0,0005	142	0.726917
original	RP1_SrNd_29	5.40–5.45	0,0006	156	0.72507
repeat			0,0009	151	0.725135

Table S3: Input data for sediment mixing models from slates of the Rhenish Massif and Pleistocene Periglacial Slope Deposits (PPSD) (Moragues-Quiroga et al., 2017).

Site	Identifier	Material	Sr [ppm]	Nd [ppm]	$^{87}Sr/^{86}Sr$	εNd
Rhenish Massif	SP1	Saprolith	96	43.11	0.741	-13.21
Rhenish Massif	SP2	Saprolith	81	35.83	0.742	-13.87
Rhenish Massif	SP3	Saprolith	102	45.39	0.739	-13.25
Rhenish Massif	SP4	Saprolith	113	59.72	0.739	-12.78
Rhenish Massif	SP5	Paralith	98	37.89	0.742	-13.75
Rhenish Massif	PPSD2	Cambic	94	37.48	0.734	-13.97
Rhenish Massif	PPSD3	Regolith	110	42.35	0.739	-13.95
Rhenish Massif	PPSD4	Regolith	126	54.1	0.737	-13.79

Table S4: Input data for sediment mixing models from the suspended load of the Rhine river (Sr and Nd isotopes and Nd concentration by Tricca et al., (1999), Bi-monthly Sr concentration data (mean) from January 2011 to December 2016 (van der Perk and Vilches, 2020).

Site	Identifier	Material	Sr [ppm]	Nd [ppm]	$^{87}Sr/^{86}Sr$	εNd
Rhine	3575:Rhine	Susp. residue			0.720	
Rhine	RESrSusp4029r4rRhine	Susp. residue				-9.32
Rhine	4029r4residue	Susp. residue		11.10		
Rhine		Susp. Sed.	194.65			

.

Table S5: Input data for sediment mixing models from volcanic rocks of the Odenwald (Siebel et al., 2012).

Site	Identifier	Material	Sr [ppm]	Nd [ppm]	$^{87}Sr/^{86}Sr$	εNd
Odenwald	SEE	flasergranitoid	207	11.9	0.709	-5.13

Table S6: Input data for sediment mixing models from the Laacher See Tephra as endmember for mantle derived material (Wörner et al., 1985).

Site	Identifier	Material	Sr [ppm]	Nd [ppm]	$^{87}Sr/^{86}Sr$	εNd
Eifel		Laacher See Tephra	500	49	0.705	-0.35

S.5 Grainsize and weathering effects on Sr and Nd isotopes

Grainsize sorting and weathering effects are well known to potentially change the original Sr isotopic composition of sediments, whereas the impact of both factors on εNd may be low to absent (cf. (Eisenhauer et al., 1999; Tütken et al., 2002; Feng et al., 2009). For the Schwalbenberg, we tested these relationships. Overall, the Sr isotope ratios (cf. S5) tend to depend on weathering and grainsize in the clay and sand fractions (note that we used bulk sediment samples, not separated for their grainsize fractions). In contrast, there is no evidence for a considerable dependency between εNd, weathering and grainsize in our dataset (cf. S6), supporting the application of εNd as a robust provenance tool at the Schwalbenberg.

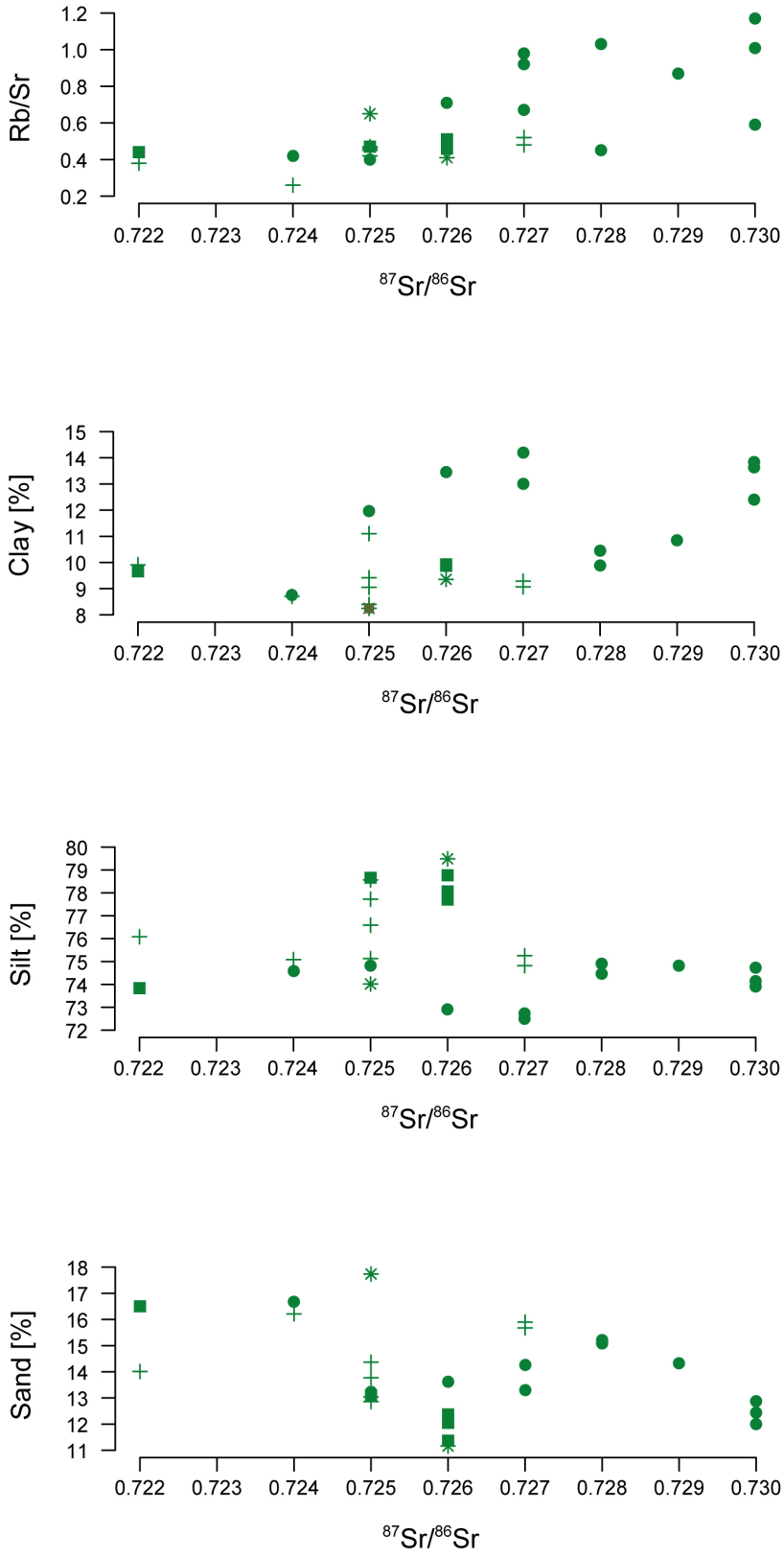

Fig. S5: Biplots showing the relationship between weathering (Rb/Sr; uppermost graph) and selected grainsize fractions to the Sr isotopic composition at the Schwalbenberg. The higher the degree of weathering or percentage of clay, the more radiogenic the Sr isotopic composition of samples tend to be ($r^2 = 0.33$ between clay and $^{87/86}Sr$), potentially limiting the use of $^{87/86}Sr$, especially in Calcaric Cambisol (Symbology: Calcaric Cambisols (●), Gelic Gleysols (■), loess (+) and reworked loess sections (✳)). No linear relationship between silt and $^{87/86}Sr$ is evident ($r^2 = 0.06$). In contrast, a weak negative relationship between sand and $^{87/86}Sr$ ($r^2 = 0.10$) can be observed.

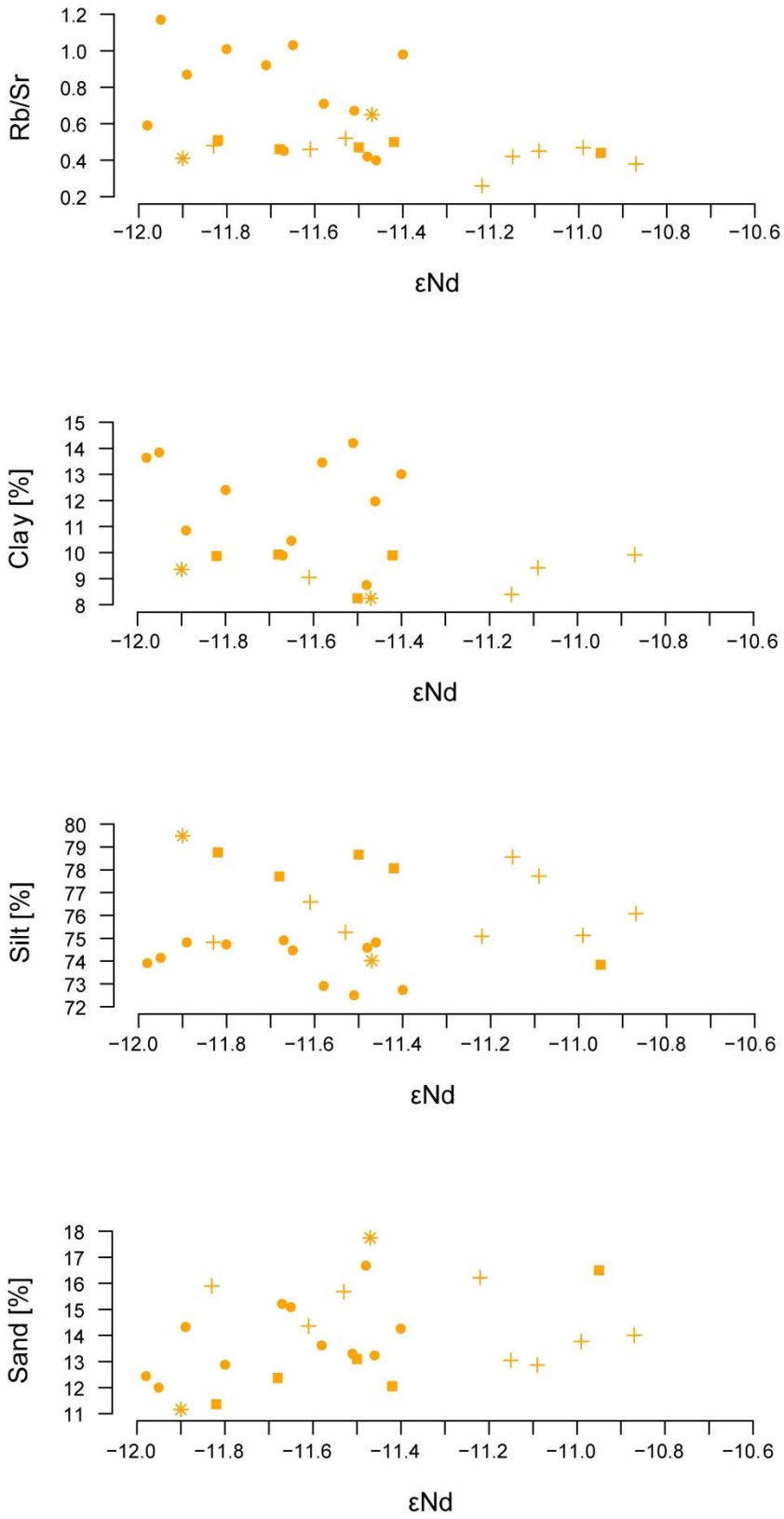

Fig. S6: Biplots showing the relationship between weathering (Rb/Sr; uppermost graph) and selected grainsize fractions to the Nd isotopic composition at the Schwalbenberg. No obvious relationship can be oberserved between weathering, grainsize and εNd (Symbology: Calcaric Cambisols (●), Gelic Gleysols (■), loess (+) and reworked loess sections (✳)) supporting the application of εNd as a sophisticated and robust provenance tool.

References

Asahara, Y., Tanaka, T., Kamioka, H., Nishimura, A., and Yamazaki, T.: Provenance of the north Pacific sediments and process of source material transport as derived from Rb–Sr isotopic systematics, Chemical Geology, 158, 271–291, https://doi.org/10.1016/S0009-2541(99)00056-X, 1999.

Bradák, B., Seto, Y., Chadima, M., Kovács, J., Tanos, P., Újvári, G., and Hyodo, M.: Magnetic fabric of loess and its significance in Pleistocene environment reconstructions, Earth-Science Reviews, 210, 103385, https://doi.org/10.1016/j.earscirev.2020.103385, 2020.

Eisenhauer, A., Meyer, H., Rachold, V., Tütken, T., Wiegand, B., Hansen, B. T., Spielhagen, R. F., Lindemann, F., and Kassens, H.: Grain size separation and sediment mixing in Arctic Ocean sediments: evidence from the strontium isotope systematic, Chemical Geology, 158, 173–188, https://doi.org/10.1016/S0009-2541(99)00026-1, 1999.

Feng, J.-L., Zhu, L.-P., Zhen, X.-L., and Hu, Z.-G.: Grain size effect on Sr and Nd isotopic compositions in eolian dust: Implications for tracing dust provenance and Nd model age, Geochem. J., 43, 123–131, https://doi.org/10.2343/geochemj.1.0007, 2009.

Hus, J. J.: The magnetic fabric of some loess/palaeosol deposits, Physics and Chemistry of the Earth, Parts A/B/C, 28, 689–699, https://doi.org/10.1016/S1474-7065(03)00128-1, 2003.

Jelinek, V.: Characterization of the magnetic fabric of rocks, Tectonophysics, 79, T63–T67, https://doi.org/10.1016/0040-1951(81)90110-4, 1981.

Költringer, C., Bradák, B., Stevens, T., Almqvist, B., Banak, A., Lindner, M., Kurbanov, R., and Snowball, I.: Palaeoenvironmental implications from Lower Volga loess - Joint magnetic fabric and multi-proxy analyses, Quaternary Science Reviews, 267, 107057, https://doi.org/10.1016/j.quascirev.2021.107057, 2021.

Lagroix, F. and Banerjee, S. K.: The regional and temporal significance of primary aeolian magnetic fabrics preserved in Alaskan loess, Earth and Planetary Science Letters, 225, 379–395, https://doi.org/10.1016/j.epsl.2004.07.003, 2004.

Moragues-Quiroga, C., Juilleret, J., Gourdol, L., Pelt, E., Perrone, T., Aubert, A., Morvan, G., Chabaux, F., Legout, A., Stille, P., and Hissler, C.: Genesis and evolution of regoliths: Evidence from trace and major elements and Sr-Nd-Pb-U isotopes, CATENA, 149, 185–198, https://doi.org/10.1016/j.catena.2016.09.015, 2017.

van der Perk, M. and Vilches, A. E.: Compositional dynamics of suspended sediment in the Rhine River: sources and controls, J Soils Sediments, 20, 1754–1770, https://doi.org/10.1007/s11368-019-02490-5, 2020.

Rees, A. I.: The Effect of Depositional Slopes on the Anisotropy of Magnetic Susceptibility of Laboratory Deposited Sands, The Journal of Geology, 74, 856–867, https://doi.org/10.1086/627216, 1966.

Siebel, W., Eroğlu, S., Shang, C. K., and Rohrmüller, J.: Zircon geochronology, elemental and Sr-Nd isotope geochemistry of two Variscan granitoids from the Odenwald-Spessart crystalline complex (mid-German crystalline rise), Miner Petrol, 105, 187–200, https://doi.org/10.1007/s00710-012-0200-3, 2012.

Tarling, D. H. and Hrouda, F.: The magnetic anisotropy of rocks, 1st ed., Chapman & Hall, London ; New York, 217 pp., 1993.

Taylor, S. N. and Lagroix, F.: Magnetic anisotropy reveals the depositional and postdepositional history of a loess-paleosol sequence at Nussloch (Germany): AMS OF NUSSLOCH LOESS-PALEOSOL SEQUENCE, J. Geophys. Res. Solid Earth, 120, 2859–2876, https://doi.org/10.1002/2014JB011803, 2015.

Tricca, A., Stille, P., Steinmann, M., Kiefel, B., Samuel, J., and Eikenberg, J.: Rare earth elements and Sr and Nd isotopic compositions of dissolved and suspended loads from small river systems in the Vosges mountains (France), the river Rhine and groundwater, Chemical Geology, 160, 139–158, https://doi.org/10.1016/S0009-2541(99)00065-0, 1999.

Tütken, T., Eisenhauer, A., Wiegand, B., and Hansen, B. T.: Glacial–interglacial cycles in Sr and Nd isotopic composition of Arctic marine sediments triggered by the Svalbard/Barents Sea ice sheet, Marine Geology, 182, 351–372, https://doi.org/10.1016/S0025-3227(01)00248-1, 2002.

Wörner, G., Staudigel, H., and Zindler, A.: Isotopic constraints on open system evolution of the Laacher See magma chamber (Eifel, West Germany), Earth and Planetary Science Letters, 75, 37–49, https://doi.org/10.1016/0012-821X(85)90048-2, 1985.

Zeeden, C. and Hambach, U.: Magnetic Susceptibility Properties of Loess From the Willendorf Archaeological Site: Implications for the Syn/Post-Depositional Interpretation of Magnetic Fabric, Front. Earth Sci., 8, 599491, https://doi.org/10.3389/feart.2020.599491, 2021.

Zhu, R., Liu, Q., and Jackson, M. J.: Paleoenvironmental significance of the magnetic fabrics in Chinese loess-paleosols since the last interglacial (<130 ka), Earth and Planetary Science Letters, 221, 55–69, https://doi.org/10.1016/S0012-821X(04)00103-7, 2004.

Zhu, R., Liu, Q., and Jackson, M. J.: Paleoenvironmental significance of the magnetic fabrics in Chinese loess-paleosols since the last interglacial (<130 ka), Earth and Planetary Science Letters, 221, 55–69, https://doi.org/10.1016/S0012-821X(04)00103-7, 2004.